Large-chiral-number corner modes in ℤ-class higher-order topolectrical circuits

Yi Li,[1,2] Jia-Hui Zhang ,[1,2] Feng Mei ,[1,2,*] Biye Xie ,[3,†] Ming-Hui Lu,[4,5,‡] Jie Ma,[1,2,§]
Liantuan Xiao,[1,2] and Suotang Jia[1,2]

[1] *State Key Laboratory of Quantum Optics and Quantum Optics Devices, Institute of Laser Spectroscopy, Shanxi University, Taiyuan, Shanxi 030006, China*

[2] *Collaborative Innovation Center of Extreme Optics, Shanxi University, Taiyuan, Shanxi 030006, China*

[3] *School of Science and Engineering, The Chinese University of Hong Kong, Shenzhen, Guangdong, 100190, China*

[4] *College of Engineering and Applied Sciences and National Laboratory of Solid State Microstructures, Nanjing University, Nanjing 210093, China*

[5] *National Laboratory of Solid State Microstructures, Collaborative Innovation Center of Advanced Microstructures, Nanjing University, Nanjing, 518172, China*

Topological corner states are exotic topological boundary states bounded to zero-dimensional geometry even when the dimension of bulk systems is larger than one. So far, all previous realizations of higher-order topological insulators (HOTI) phases are hallmarked by $\mathbb{Z}_2$ topological invariants and therefore have only one corner state at each corner. Here, we report an experimental demonstration of $\mathbb{Z}$-class HOTI phases in electrical circuits, characterized by multipole chiral numbers N, hosting large-number corner modes at each corner. By measuring the impedance spectra and distributions, we clearly observe that the multipole corner modes in $\mathbb{Z}$-class HOTI phases feature scalable mode areas. Moreover, we find that the local density of states (LDOS) at each corner is maximally distributed at N corner unit cells, differing conspicuously from the $\mathbb{Z}_2$-class case, where the LDOS only dominates over one corner unit cell, allowing us to probe the topological number N and reveal the corresponding fractional corner charges. Our results extend the observation of HOTIs from the $\mathbb{Z}_2$ class to the $\mathbb{Z}$ class and the coexistence of spatially overlapping large numbers of corner modes that may enable exotic topological devices that require high-degeneracy boundary states.

I. INTRODUCTION

Bulk-boundary correspondence, as one of the most important physical properties of topological materials, links the bulk topological invariant to the number of boundary states at a certain open boundary [1,2]. For $\mathbb{Z}$-class topological phases, the topological invariant is no longer limited to unity and can be a larger number, consequently generating large numbers of topological boundary states [1,2]. Besides the fundamental interest, multipole topological boundary states can significantly improve the channel capacities and coupling efficiencies, having great practical value in enabling functional topological photonic, acoustic, and mechanical devices [3–10]. Therefore, the realization of such an unusual topological phase is highly desirable but very hard. Until recently, topological

insulator phases with larger Chern numbers [11–14] have been experimentally reported in photonic crystals [15] and solid materials [16].

The recent discovery of HOTI phases has further expanded the concept of topological phases [17–20]. One appealing feature associated with such a phase is the existence of lower-dimensional topological boundary states; e.g., topological corner states of zero dimension. Topological corner states have recently attracted great interest in many platforms [21,22], such as photonics [23–32], phononics [33–47], and electrical circuits [48–62]. They have also motivated numerous important applications and studies, ranging from topological cavities and lasers [63, 64] to nonlinear [65–68] and quantum optics [69,70]. The latest finding is that HOTIs are not limited to the $\mathbb{Z}_2$ class, which can be further promoted to the $\mathbb{Z}$ class [71]. As illustrated in Figs. 1(a) and 1(b), distinct from $\mathbb{Z}_2$-class HOTI phases, $\mathbb{Z}$-class HOTI phases are classified by multipole chiral numbers (MCNs) N, featuring N corner modes at each corner [71]. However, it is quite a challenge to realize long-range couplings in photonic and phononic topological

*meifeng@sxu.edu.cn
†xiebiye@cuhk.edu.cn
‡luminghui@nju.edu.cn
§mj@sxu.edu.cn

platforms, thus hindering the experimental demonstration of such unconventional phases.

In this work, we report on the experimental realization and detection of $\mathbb{Z}$-class HOTI phases using topolectrical circuits. Going beyond previous experiments on $\mathbb{Z}_2$-class HOTI phase, the experimental implementation of $\mathbb{Z}$-class HOTI phases [71] can provide more insights into HOTI phases, such as observing multipole corner modes at each corner, demonstrating HOTI phases protected by a $\mathbb{Z}$-class topological invariant instead of the $\mathbb{Z}_2$-class, and filling the gap of the HOTI phase in the AIII class. In the past few years, electrical circuits have been demonstrated to be a powerful platform in implementing topological lattice models and exploring topological phases [48,72–74], including lattice geometry [60,75–77], higher dimensions [55,78,79], long-range couplings [59,61], gauge fields [80,81], and nonlinear [82,83] and non-Hermitian terms [84–86]. In addition to topological band structures and boundary states, this system also allows us to investigate the dynamics [87–89], the topological temporal pump [90], and nonlinear [91] and non-Hermitian physics [92].

To realize $\mathbb{Z}$-class HOTI phases, we need to design and fabricate a circuit lattice with long-range couplings. Based on calculating multipole chiral numbers N and

circuit admittance spectra, we show that our constructed long-range circuits support four distinct nontrivial $\mathbb{Z}$-class HOTI phases identified by $N = 1, 2, 3, 4$ and host N corner modes at each corner. Experimentally, the measured zero-energy corner-mode resonances and density distributions agree well with the simulated results, demonstrating the emergence of $\mathbb{Z}$-class HOTI phases in the circuits. We have also explored the mode areas of the corner modes in $\mathbb{Z}$-class HOTI phases. It turns out that, distinct from $\mathbb{Z}_2$-class HOTI phases, the mode area in the $\mathbb{Z}$-class HOTI phase scales up with the value of the MCN. Therefore, the corner modes in $\mathbb{Z}$-class HOTI phases feature scalable mode areas that could enable novel applications in designing topological corner lasers. Moreover, we implement LDOS measurements in our topolectrical circuit experiments, which provides a direct way to detect the multipole chiral number N, i.e., the $\mathbb{Z}$-class topological invariants established in real space for classifying $\mathbb{Z}$-class HOTI phases [71], thus making different $\mathbb{Z}$-class HOTI phases experimentally distinguishable. Furthermore, we find that LDOS measurements also allow us to gain more insights into the fractional corner charges in $\mathbb{Z}$-class HOTI phases. Different from $\mathbb{Z}_2$-class HOTI phases that have a single $\frac{1}{2}$ fractional charge at each corner, our experimental results
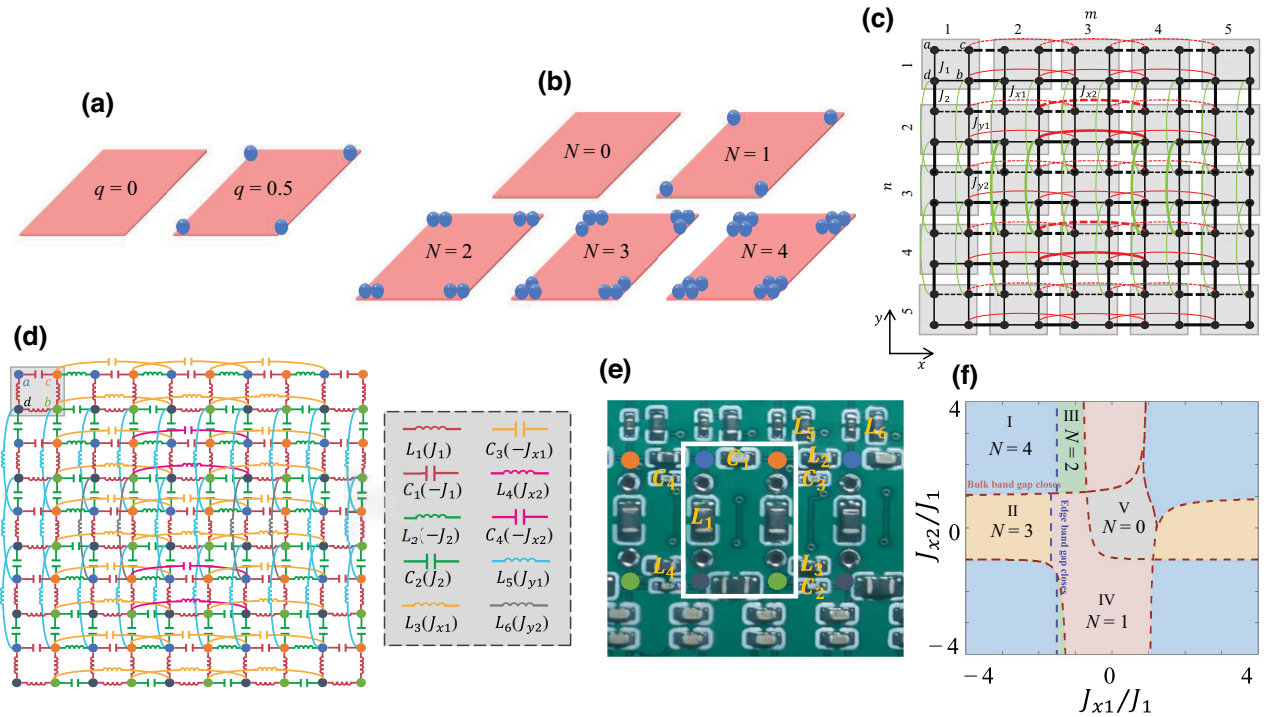

FIG. 1. (a) The $\mathbb{Z}_2$-class HOTI phases, characterized by quantized quadrupole moments, featuring one corner mode at each corner. (b) The $\mathbb{Z}$-class HOTI phases, protected by multipole chiral numbers, hosting multipole corner modes at each corner. (c) A diagram of the tight-binding lattice model with nontrivial multipole chiral numbers N, where J_1, J_2, J_{1x}, J_{2x}, J_{1y}, and J_{2y} represent different hopping strengths and the dashed lines represent hopping terms with negative sign. (d) The circuit diagram for implementing the long-range-coupling lattice model hosting $\mathbb{Z}$-class HOTI phases. The gray square lists the specific circuit elements and the corresponding lattice parameters. (e) An experimentally realized circuit for a unit cell on a printed circuit board. (f) The topological phase diagram in terms of the MCNs in the parameter space of J_{x1} and J_{x2} for $J_{y1} = J_{x1}$, $J_{y2} = J_{x2}$, and $J_2 = -0.5J_1$.

show that ℤ-class HOTI phases have N such fractional charges neatly distributed in each corner.

II. ℤ-CLASS HIGHER-ORDER TOPOLECTRICAL CIRCUITS

In Fig. 1(d), we design an electrical circuit to demonstrate its power in building long-range couplings, which is crucial and valuable for realizing and exploring various complex topological phases. The response of a circuit at frequency ω is given by Kirchhoff's law $I_a = \sum_b J_{ab}(\omega)V_b(\omega)$, where I_a is the input current flowing out of node a, $V_b(\omega)$ is the voltage of the circuit node b, and $J_{ab}(\omega)$ is the element of the circuit Laplacian. At the resonant frequency, the circuit Laplacian functions as the analogue of the lattice-model Hamiltonian, with the circuit nodes being the lattice sites.

The tight-binding lattice model that we implement in this work by using electrical circuits is shown in Fig. 1(c). The total Hamiltonian constitutes two parts, described by $H = H_{\text{BBH}} + H_{\text{LRC}}$, where H_{BBH} and H_{LRC} are, respectively, the Benalcazar-Bernevig-Hughes– (BBH) model Hamiltonian and the dimerized long-range-couplings Hamiltonian, written as

$$
\begin{aligned}
H_{\text{BBH}} = {} & J_1 \sum_{m,n} (-a^\dagger_{m,n} c_{m,n} + d^\dagger_{m,n} a_{m,n} + b^\dagger_{m,n} d_{m,n} + c^\dagger_{m,n} b_{m,n} + \text{h.c.}) \\
& + J_2 \sum_{m,n} (-a^\dagger_{m,n} c_{m-1,n} - c^\dagger_{m,n} a_{m+1,n} + d^\dagger_{m,n} a_{m,n+1} + a^\dagger_{m,n} d_{m,n-1} \\
& + b^\dagger_{m,n} d_{m+1,n} + d^\dagger_{m,n} b_{m-1,n} + c^\dagger_{m,n} b_{m,n-1} + b^\dagger_{m,n} c_{m,n+1}), \\
H_{\text{LRC}} = {} & \sum_{m \in \text{even}} \sum_n (J_x + (-1)^n \delta_x) \left(-a^\dagger_{m,n} c_{m-2,n} - c^\dagger_{m,n} a_{m+2,n} + b^\dagger_{m,n} d_{m+2,n} + d^\dagger_{m,n} b_{m-2,n}\right) \\
& + \sum_m \sum_{n \in \text{even}} (J_y + (-1)^m \delta_y) \left(a^\dagger_{m,n} d_{m,n-2} + d^\dagger_{m,n} a_{m,n+2} + c^\dagger_{m,n} b_{m,n-2} + b^\dagger_{m,n} c_{m,n+2}\right) \\
& + J_{x1} \sum_{m \in \text{odd}} \sum_n \left(-a^\dagger_{m,n} c_{m-2,n} - c^\dagger_{m,n} a_{m+2,n} + b^\dagger_{m,n} d_{m+2,n} + d^\dagger_{m,n} b_{m-2,n}\right) \\
& + J_{y1} \sum_m \sum_{n \in \text{odd}} \left(a^\dagger_{m,n} d_{m,n-2} + d^\dagger_{m,n} a_{m,n+2} + c^\dagger_{m,n} b_{m,n-2} + b^\dagger_{m,n} c_{m,n+2}\right),
\end{aligned}
\tag{1}
$$

where the unit-cell position is labeled as (m, n), J_1 and J_2 are the dimerized nearest-neighbor couplings, $J_{x(y)} = (J_{x1(y1)} + J_{x2(y2)})/2$, and $\delta_{x(y)} = (J_{x2(y2)} - J_{x1(y1)})/2$, with J_{x1} (J_{y1}) and J_{x2} (J_{y2}) being the dimerized long-range couplings along the even x (y) direction. The long-range couplings in our work are chosen between next-nearest-neighbor unit cells but can easily be generalized to be much longer.

Specifically, as shown in Fig. 1(d), each unit cell contains four nodes labeled by a-d. The positive and negative couplings are, respectively, implemented by inductors and capacitors, as shown in Fig. 1(e) for its realization on a printed circuit board. Based on the ℤ-class HOTI model [71], we further find that as the long-range intracell couplings are designed to feature dimerized configurations in the even rows and columns, the corresponding circuit has much richer topological phase transitions, as presented in Fig. 1(f).

The long-range couplings in Fig. 1(d) are designed in a chiral-symmetry fashion. Thus, the circuit lattice naturally inherits chiral symmetry and its ℤ-class higher-order bulk topology is characterized by the MCN [71], which is a real-space topological invariant, defined as

$$
N = \frac{1}{2\pi i} \text{Tr} \log(\bar{Q}^A_{xy} \bar{Q}^{B\dagger}_{xy}),
\tag{2}
$$

where $\bar{Q}^{A,B}_{xy}$ are the multipole moment operators projected into the sublattice spaces. By numerically calculating the MCN, the topological phase diagram associated with the implemented lattice-model Hamiltonian in Fig. 1(c) is presented in Fig. 1(f). The result shows that the presence of long-range couplings could drive the circuit into four distinct nontrivial ℤ-class HOTI phases, as indicated by $N = 1, 2, 3, 4$. There are two different topological phase transitions in this system, as labeled in Fig. 1(f) in the phase boundaries, accompanied, respectively, by the bulk and edge band-gap closings. In particular, implementing the ℤ-class HOTI phase $N = 3$ in our model does not require complicated diagonal long-range couplings [71].

Moreover, for the nontrivial cases $N > 1$, the corresponding system features the trivial quadrupole moment $q = 0$. However, as shown below, they indeed host large-number topological corner modes, satisfying bulk-corner correspondences.

To demonstrate the emergence of multipole corner modes in the circuits, in Figs. 2(a)–2(d) we simulate the eigenvalues of the circuit Laplacians varying with the driving frequency, for circuits featuring different MCNs. The grounding conditions (see Sec. II in the Supplemental Material [93]) are taken into account in the simulations so that all diagonal terms in the circuit Laplacian vanish at the resonant frequencies. As manifested, the corresponding spectra respect chiral symmetry at the resonant frequencies $f_0 = 876$ kHz for $N = 1, 2, 4$ and $f_0 = 1591$ kHz for $N = 3$. By sorting them out in Figs. 2(e)–2(h), we can see that the circuit Laplacians support large numbers of gapped zero modes, with their specific numbers given by $4N$, determined by the MCNs. Figures 2(i)–2(l) plot the corresponding distributions in the circuit lattices for these zero modes, which maximum distribute at corner sites, indicating that they are corner modes, together with Figs. 2(e)–2(h) confirming the $\mathbb{Z}$-class higher-order bulk-corner correspondences. Compared to $\mathbb{Z}_2$-class HOTI

phases, the corner modes in the $\mathbb{Z}$-class HOTI phases have much larger mode areas and richer distribution features. For example, Figs. 2(i)–2(l) show that as N increases from 1 to 4, the corner-mode area could increase from 1 unit cell to roughly 16 unit cells, which may can motivate novel applications in designing topological corner-mode lasers.

III. OBSERVING LARGE-NUMBER CORNER MODES WITH SCALABLE MODE AREAS

We experimentally fabricate four nontrivial $\mathbb{Z}$-class higher-order topolectrical circuits, corresponding to $N = 1, 2, 3, 4$, respectively. Their featured higher-order topological features, i.e., the zero-energy corner-mode resonances and density distributions (as predicted in Fig. 2), are detected by measuring the impedance Z_a between the node a and the ground, which is related to the eigenvalues and eigenvectors of the circuit Laplacian, j_n and ψ_n, respectively, via $Z_a = \sum_n |\psi_{n,a}|^2 / j_n$. This relationship enables, when the circuit is excited at the resonant frequency, that the impedances at the corner nodes should be extremely large compared to the impedances at the bulk and edge nodes, as in the corner nodes zero-energy corner modes have been excited mostly, which leads to the fact that
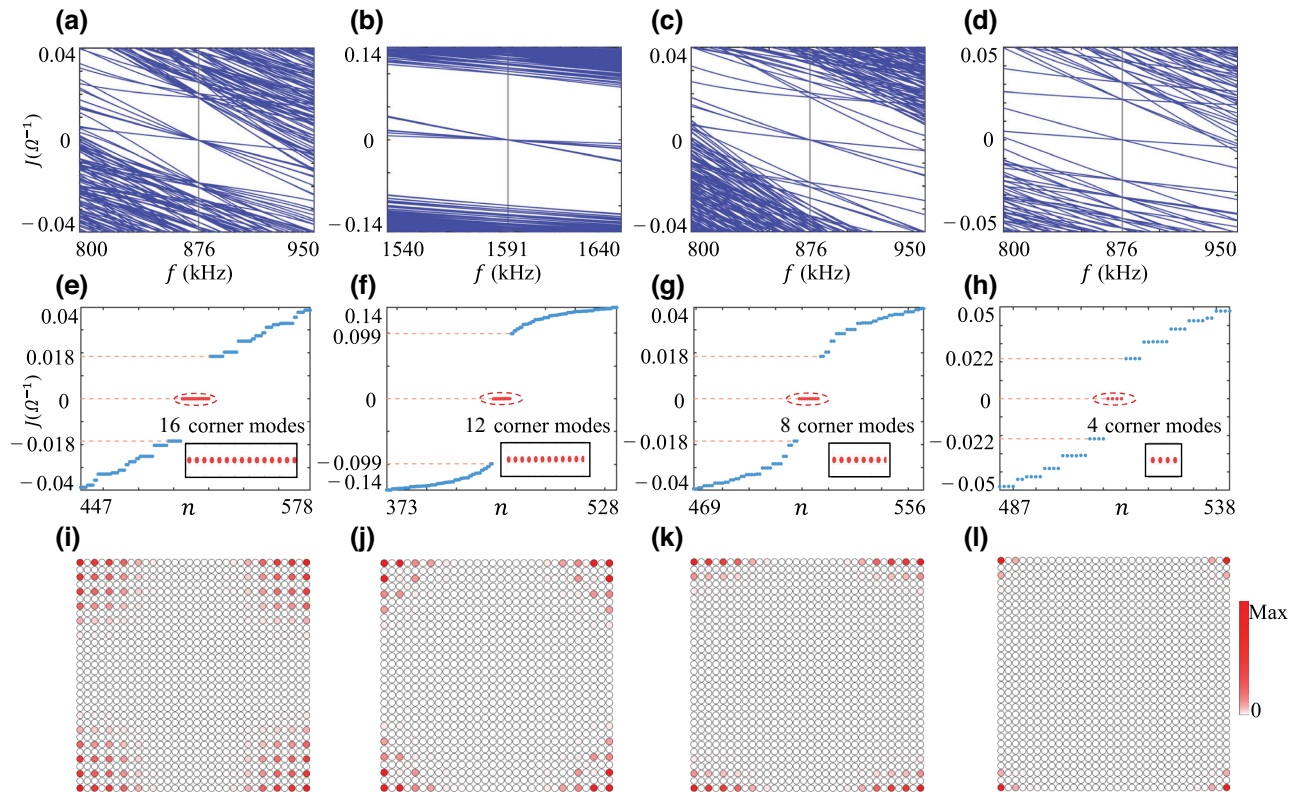

FIG. 2. The large-number corner modes that emerge in circuit Laplacian spectra. (a)–(d) Simulated admittance spectra as a function of the driving frequency for different MCNs: (a),(e) $N = 4$; (b),(f) $N = 3$; (c),(g) $N = 2$; (d),(h) $N = 1$. At the resonant frequencies (gray solid lines), the spectra respect chiral symmetry (red dashed lines) and host large-number ($4N$) zero modes that correspond to corner modes, as manifested by sorting them out in (e)–(h). (i)–(l) The simulated distributions of the zero-energy corner modes, revealing that the corner modes in $\mathbb{Z}$-class HOTI phases have extended mode areas.
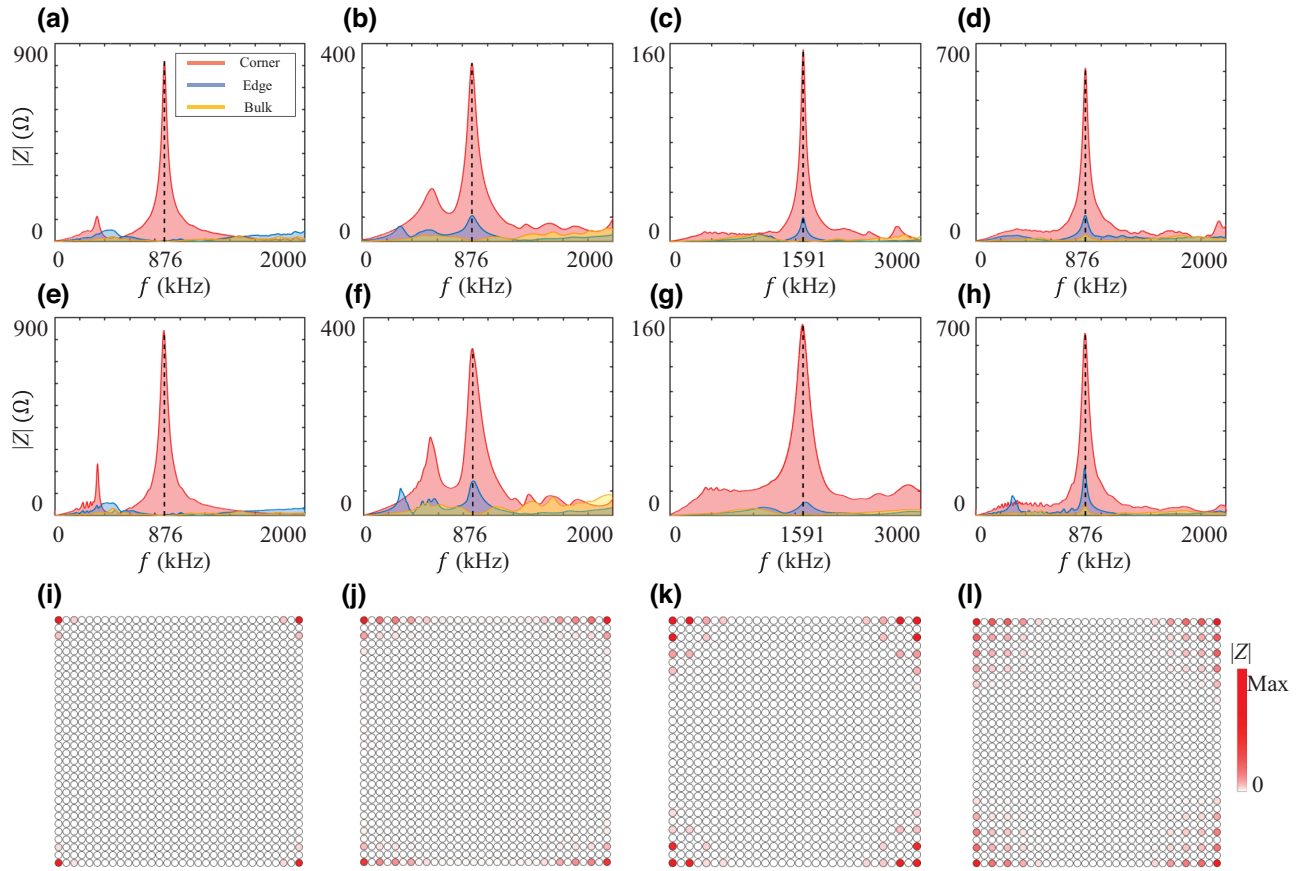
FIG. 3. The observation of large-number corner modes featuring scalable mode areas. The (a)–(d) simulated and (e)–(h) measured impedances between the corner, edge, and bulk circuit nodes and the ground via scanning the driving frequency in different ℤ-class higher-order topological circuits: (a),(e) $N = 1$; (b),(f) $N = 2$; (c),(g) $N = 3$; (d),(h) $N = 4$. Both results clearly verify that the corner-mode resonances occur at the resonant frequencies (black dashed lines). (i)–(l) The measured impedance distributions for the corner modes, demonstrating that the mode areas in the ℤ-class HOTI phases scale up with the MCNs.

$|\psi_{n,a}|^2$ is maximal and j_n is near zero at corners. Figures 3(a)–3(d) verify this feature for four different MCNs based on simulating the measurements using the LTspice simulation software. As expected, the highest peaks in the simulated corner impedances occur at the resonant frequencies and the small peaks in the edge impedances reflect that the distribution of the corner modes extends to edge nodes in the ℤ-class HOTI phases with larger MCNs. The experimentally measured corner, edge, and bulk impedances are presented in Figs. 3(e)–(h), respectively, for different MCNs, and agree very well with the simulation results. In circuit systems, the broadening around the resonant frequency is due to the parasitic resistance of the inductors. In practical experiments, the inductor resistances increase with the driven frequency of the circuit. Then, there exists a considerable broadening in the $N = 3$ phase, which has a larger resonant frequency. The distributions of the corner modes in the circuits are probed by measuring the all-node impedances at the resonant frequencies. As displayed in Figs. 3(i)–3(l), as the topological invariant N increases from 1 to 4, the corner-mode areas will extend to the edge

and bulk nodes, scaling up with the MCNs, in accordance with the theoretical simulations in Figs. 2(i)–2(l).

IV. PROBING MCNs AND REVEALING FRACTIONAL CORNER CHARGES

To unambiguously distinguish the different ℤ-class HOTI phases, it is highly desirable to have the capability to detect the MCN values. The simplest way is to count the numbers of corner modes that equal the MCNs according to bulk-corner correspondence. However, the corner modes are degenerate in the admittance spectra and cannot be extracted. We now show that such topological numbers can be probed by LDOS measurements. Note that the use of LDOS measurements to probe fractional charges has recently attracted great interest in photonic and acoustic systems [94–99]. For circuit systems, the LDOS (mode density) at each circuit node—e.g., the circuit node a—is measured via the real part of the impedance Z_a, i.e., $\rho(f, a) = 2f \, \mathrm{Re}[Z_a]$ (see Sec. IV in the Supplemental Material [93]). In Fig. 4, we exemplify the ℤ-class
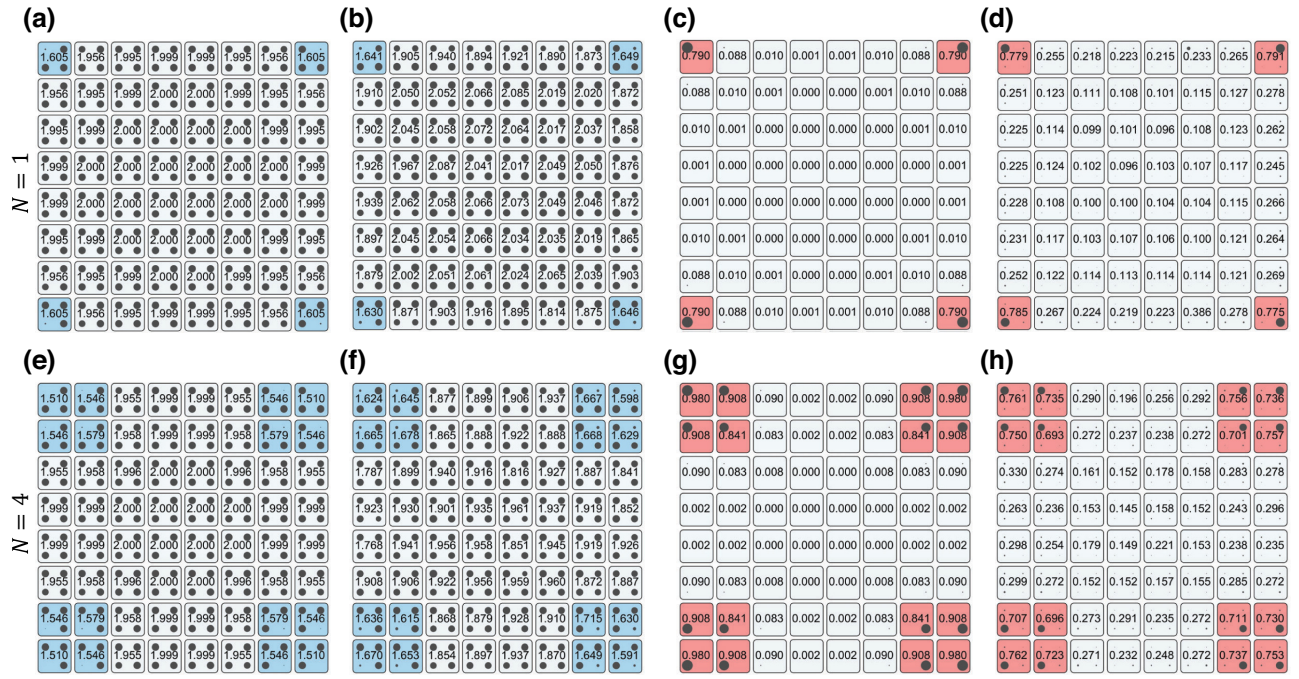
FIG. 4. Spatial maps of simulated and measured LDOSs for $N = 1$ and $N = 4$ integrating over (a),(b),(e),(f) the lower band and (c),(d),(g),(h) an in-gap spectral range covering all corner modes: (a),(e) simulated; (b),(f) measured; (c) four corner modes, simulated; (d) four corner modes, measured; (g) 16 corner modes, simulated; (h) 16 corner modes, measured. Each circuit node is represented as a circle with a radius proportional to the LDOS. Each number gives the LDOS in the corresponding unit cell. The topological invariants N and fractional corner charges are, respectively, detected and manifested by the LDOSs in the shaded corner unit cells.

topological phases $N = 1$ and $N = 4$. To extract the MCNs from the LDOS, the LDOS for each unit cell has been integrated over the lower band [Figs. 4(a), 4(b), 4(e), and 4(f)] and an in-gap spectral range taking into account all corner modes [Figs. 4(c), 4(d), 4(g), and 4(h)]. As shown, the experimentally measured data agree well with the theoretically simulated results.

According to the bulk-corner correspondence, the value of the MCN is equal to the number of corner modes at each corner. The number of corner modes can be measured by summing the in-gap LDOSs over all unit cells. Consequently, there exists a direct relationship between the MCN and the in-gap LDOS, $N = \sum_r \rho_r^{\text{gap}}/4$, where r is the unit-cell index. Unfortunately, due to experimental imperfections (see Sec. V in the Supplemental Material [93]), we are unable to precisely measure the value of the in-gap LDOS and thus we cannot extract the value of the MCN using the above relationship. However, we still can infer the MCN from the number of unit cells with a maximally distributed LDOS, which evidences the numbers of corner modes. Specifically, such unit cells are referred to as corner-localized unit cells (marked by shaded backgrounds in Fig. 4). For the in-gap LDOS, contributed solely by the corner modes, each bulk unit cell features almost zero value and only the corner LDOS dominates, in accordance with the theoretical expectation. As the corner modes have weights in the edge and bulk nodes, the in-gap LDOS ρ_c^{gap}

in the shaded corner unit cells is closing to but not equal to 1 but the numbers of such corner-localized unit cells can still manifest the numbers of corner modes, i.e., the value of the MCN. Given the obvious difference between the LDOS in the corner-localized unit cells and the rest of the unit cells, such an indicator is a robust observable for experimental detection.

The value of the MCN can also be inferred from the lower-band LDOS. From Figs. 4(a), 4(b), 4(e), and 4(f), we see that the measured lower-band LDOS in each bulk unit cell is approximately $\rho = 2$, which conforms to the expectation at half filling (the lower band is twofold degenerate). In contrast, the lower-band LDOSs ρ_c^{band} in the shaded corner unit cells are no longer 2, due to the in-gap corner modes that are occupying them. More specifically, for $N = 4$, at each corner there are 4 corner unit cells within which the LDOS is closing to 1.5, while for $N = 1$ there is only one such unit cell. Similarly to the case in the lower-band LDOSs, the numbers of corner-localized unit cells in the in-gap LDOSs also reflect the numbers of corner modes, i.e., the MCN. Moreover, we can observe that the difference between the bulk and corner lower-band LDOSs is due to the presence of the corner mode at the corner unit cell. With this feature, the corner-mode charge can be inferred as $1/2$, agreeing with the results reported in two recent acoustic experiments [97,99]. For the $\mathbb{Z}$-class topological phases $N = 4$, we also find that there are four $\frac{1}{2}$

fractional corner charges distributed at each corner, which is distinct from the $\mathbb{Z}_2$-class topological phases hosting one such fractional corner charge.

V. CONCLUSIONS

In summary, we have experimentally realized $\mathbb{Z}$-class HOTI phases in electrical circuits. Distinct from the intensively studied $\mathbb{Z}_2$-class HOTI phase, the recently theoretically established $\mathbb{Z}$-class HOTI phases [71] are protected by $\mathbb{Z}$-class topological invariant and feature multipole corner modes at each corner. By fabricating long-range-coupling topolectrical circuits and measuring the impedances in all circuit nodes, we have realized four distinct $\mathbb{Z}$-class HOTI phases characterized by MCNs with $N = 1, 2, 3, 4$, we have detected the corresponding zero-energy corner-mode resonances, and we have revealed that the corner modes in $\mathbb{Z}$-class HOTI phases have much larger mode areas, scaling up with the MCN N. Additionally, based on LDOS measurements, we have further probed the values of N, making the different $\mathbb{Z}$-class HOTI phases experimentally distinguishable. With the same LDOS data, we have also found that there are N fractional corner charges $\frac{1}{2}$, distributed in an orderly manner at each corner. As shown, our experiment has not only demonstrated the theoretically predicted $\mathbb{Z}$-class HOTI phases [71] but also provided a method to detect the topologically invariant MCN and reveal the fractional charges associated with the multipole corner modes. Therefore, our work will hopefully promote further theoretical and experimental studies on HOTI phases.

The realization of large topological numbers and multipole corner modes in one corner structure will have several important consequences. First, a higher-order topological pump [100,101] has recently been achieved based on $\mathbb{Z}_2$ HOTI phases. However, with our observed $\mathbb{Z}_2$ HOTI phases, four corner states at each corner feature degenerate evolution and may lead to a non-Abelian topological pump [102]. Second, the creation of a disclination structure from our lattice can trap large-number degenerate topological disclination states at the disclination core, thus going beyond previous $\mathbb{Z}_{\neq}$ topological disclination states [103–105]. Third, when gain and loss are introduced into our circuits [84,85,92], one can study $\mathcal{PT}$-symmetry phase transitions [106,107] in our circuit lattices. Due to the four corner states at each corner, the non-Hermitian HOTI phase diagram might be more diverse than its $\mathbb{Z}_2$-class counterpart. Finally, the large-number corner modes with scalable mode areas may hold promise for enabling exotic topological lasers [63,64].

ACKNOWLEDGMENTS

[1] M. Z. Hasan and C. L. Kane, Colloquium: Topological insulators, Rev. Mod. Phys. **82**, 3045 (2010).

[2] X. L. Qi and S. C. Zhang, Topological insulators and superconductors, Rev. Mod. Phys. **83**, 1057 (2011).

[3] L. Lu, J. D. Joannopoulos, and M. Soljačić, Topological photonics, Nat. Photonics **8**, 821 (2014).

[4] S. D. Huber, Topological mechanics, Nat. Phys. **12**, 621 (2016).

[5] A. B. Khanikaev and G. Shvets, Two-dimensional topological photonics, Nat. Photonics **11**, 763 (2017).

[6] X. Zhang, M. Xiao, Y. Cheng, M. H. Lu, and J. Christensen, Topological sound, Commun. Phys. **1**, 97 (2018).

[7] T. Ozawa, H. M. Price, A. Amo, N. Goldman, M. Hafezi, L. Lu, C. R. Mikael, S. David, S. Jonathan, Z. Oded, and C. Iacopo, Topological photonics, Rev. Mod. Phys. **91**, 015006 (2019).

[8] G. Ma, M. Xiao, and C. T. Chan, Topological phases in acoustic and mechanical systems, Nat. Rev. Phys. **1**, 281 (2019).

[9] H. Xue, Y. Yang, and B. Zhang, Topological acoustics, Nat. Rev. Mater. **7**, 974 (2022).

[10] X. Ni, S. Yves, A. Krasnok, and A. Alu, Topological metamaterials, Chem. Rev. **12**, 2023 (7585).

[11] J. Wang, B. Lian, H. Zhang, Y. Xu, and S. C. Zhang, Quantum anomalous Hall effect with higher plateaus, Phys. Rev. Lett. **111**, 136801 (2013).

[12] C. Fang, M. J. Gilbert, and B. A. Bernevig, Large-Chern-number quantum anomalous Hall effect in thin-film topological crystalline insulators, Phys. Rev. Lett. **112**, 046801 (2014).

[13] T. S. Xiong, J. Gong, and J. H. An, Towards large-Chern-number topological phases by periodic quenching, Phys. Rev. B **93**, 184306 (2016).

[14] S. A. Skirlo, L. Lu, and M. Soljačić, Multimode one-way waveguides of large Chern numbers, Phys. Rev. Lett. **113**, 113904 (2014).

[15] S. A. Skirlo, L. Lu, Y. Igarashi, Q. Yan, J. Joannopoulos, and M. Soljačić, Experimental observation of large Chern numbers in photonic crystals, Phys. Rev. Lett. **115**, 253901 (2015).

[16] Y. F. Zhao, R. Zhang, R. Mei, L. J. Zhou, H. Yi, Y. Q. Zhang, J. Yu, R. Xiao, K. Wang, N. Samarth, M. H. W. Chan, C. X. Liu, and C. Z. Chang, Tuning the Chern number in quantum anomalous Hall insulators, Nature **588**, 419 (2020).

[17] W. A. Benalcazar, B. A. Bernevig, and T. L. Hughes, Quantized electric multipole insulators, Science **357,** 61 (2017).

[18] J. Langbehn, Y. Peng, L. Trifunovic, F. von Oppen, and P. W. Brouwer, Reflection-symmetric second-order topological insulators and superconductors, Phys. Rev. Lett. **119,** 246401 (2017).

[19] Z. Song, Z. Fang, and C. Fang, $(d-2)$-dimensional edge states of rotation symmetry protected topological states, Phys. Rev. Lett. **119,** 246402 (2017).

[20] F. Schindler, A. M. Cook, M. G. Vergniory, Z. Wang, S. S. Parkin, B. A. Bernevig, and T. Neupert, Higher-order topological insulators, Sci. Adv. **4,** eaat0346 (2018).

[21] B. Xie, H.-X. Wang, X. Zhang, P. Zhan, J.-H. Jiang, M. Lu, and Y. Chen, Higher-order band topology, Nat. Rev. Phys. **3,** 520 (2021).

[22] M. Kim, Z. Jacob, and J. Rho, Recent advances in 2D, 3D and higher-order topological photonics, Light Sci. Appl. **9,** 130 (2020).

[23] C. W. Peterson, W. A. Benalcazar, T. L. Hughes, and G. Bahl, A quantized microwave quadrupole insulator with topologically protected corner states, Nature **555,** 346 (2018).

[24] J. Noh, W. A. Benalcazar, S. Huang, M. J. Collins, K. P. Chen, T. L. Hughes, and M. C. Rechtsman, Topological protection of photonic mid-gap defect modes, Nat. Photonics **12,** 408 (2018).

[25] A. E. Hassan, F. K. Kunst, A. Moritz, G. Andler, E. J. Bergholtz, and M. Bourennane, Corner states of light in photonic waveguides, Nat. Photonics **13,** 697 (2019).

[26] B. Y. Xie, G. X. Su, H. F. Wang, H. Su, X. P. Shen, P. Zhan, M.-H. Lu, Z. -L. Wang, and Y.-F. Chen, Visualization of higher-order topological insulating phases in two-dimensional dielectric photonic crystals, Phys. Rev. Lett. **122,** 233903 (2019).

[27] X. D. Chen, W. M. Deng, F. L. Shi, F. L. Zhao, M. Chen, and J. W. Dong, Direct observation of corner states in second-order topological photonic crystal slabs, Phys. Rev. Lett. **122,** 233902 (2019).

[28] S. Mittal, V. V. Orre, G. Zhu, M. A. Gorlach, A. Poddubny, and M. Hafezi, Photonic quadrupole topological phases, Nat. Photonics **13,** 692 (2019).

[29] B. Xie, G. Su, H.-F. Wang, F. Liu, L. Hu, S.-Y. Yu, P. Zhan, M.-H. Lu, Z.-L Wang, and Y.-F. Chen, Higher-order quantum spin Hall effect in a photonic crystal, Nat. Commun. **11,** 3768 (2020).

[30] Y. Wang, B. Y. Xie, Y. H. Lu, Y. J. Chang, H. F. Wang, J. Gao, Z.-Q. Jiao, Z. Feng, X.-Y. Xu, F. Mei, S. Jia, M.-H. Lu, and X.-M. Jin, Quantum superposition demonstrated higher-order topological bound states in the continuum, Light Sci. Appl. **10,** 173 (2021).

[31] J. Schulz, J. Noh, W. A. Benalcazar, G. Bahl, and G. von Freymann, Photonic quadrupole topological insulator using orbital-induced synthetic flux, Nat. Commun. **13,** 6597 (2022).

[32] Y. Zhang, D. Bongiovanni, Z. Wang, X. Wang, S. Xia, Z. Hu, D. Song, D. Jukić, J. Xu, R. Morandotti, H. Buljan, and Z. Chen, Realization of photonic p-orbital higher-order topological insulators, eLight **3,** 5 (2023).

[33] M. S. Garcia, V. Peri, R. Susstrunk, O. R. Bilal, T. Larsen, L. G. Villanueva, and S. D. Huber, Observation of a phononic quadrupole topological insulator, Nature **555,** 342 (2018).

[34] H. Xue, Y. Yang, F. Gao, Y. Chong, and B. Zhang, Acoustic higher-order topological insulator on a kagome lattice, Nat. Mater. **18,** 108 (2019).

[35] X. Ni, M. Weiner, A. Alu, and A. B. Khanikaev, Observation of higher-order topological acoustic states protected by generalized chiral symmetry, Nat. Mater. **18,** 113 (2019).

[36] X. Zhang, H. X. Wang, Z. K. Lin, Y. Tian, B. Xie, M. H. Lu, Y.-F. Chen, and J.-H. Jiang, Second-order topology and multidimensional topological transitions in sonic crystals, Nat. Phys. **15,** 582 (2019).

[37] X. Zhang, B. Y. Xie, H. F. Wang, X. Xu, Y. Tian, J. H. Jiang, M. H. Lu, and Y. F. Chen, Dimensional hierarchy of higher-order topology in three-dimensional sonic crystals, Nat. Commun. **10,** 5331 (2019).

[38] H. Xue, Y. Yang, G. Liu, F. Gao, Y. Chong, and B. Zhang, Realization of an acoustic third-order topological insulator, Phys. Rev. Lett. **122,** 244301 (2019).

[39] Y. Qi, C. Qiu, M. Xiao, H. He, M. Ke, and Z. Liu, Acoustic realization of quadrupole topological insulators, Phys. Rev. Lett. **124,** 206601 (2020).

[40] X. Ni, M. Li, M. Weiner, A. Alu, and A. B. Khanikaev, Demonstration of a quantized acoustic octupole topological insulator, Nat. Commun. **11,** 2108 (2020).

[41] Y. Yang, J. Lu, M. Yan, X. Huang, W. Deng, and Z. Liu, Hybrid-order topological insulators in a phononic crystal, Phys. Rev. Lett. **126,** 156801 (2021).

[42] H. Qiu, M. Xiao, F. Zhang, and C. Qiu, Higher-order Dirac sonic crystals, Phys. Rev. Lett. **127,** 146601 (2021).

[43] S. Q. Wu, Z. K. Lin, B. Jiang, X. Zhou, Z. H. Hang, B. Hou, and J. H. Jiang, Higher-order topological states in acoustic twisted Moire superlattices, Phys. Rev. Appl. **17,** 034061 (2022).

[44] S. Zheng, X. Man, Z. L. Kong, Z. K. Lin, G. Duan, N. Chen, D. Yu, J.-H. Jiang, and B. Xia, Observation of fractal higher-order topological states in acoustic metamaterials, Sci. Bull. **67,** 2069 (2022).

[45] J. Li, Q. Mo, J. H. Jiang, and Z. Yang, Higher-order topological phase in an acoustic fractal lattice, Sci. Bull. **67,** 2040 (2022).

[46] S. Zheng, X. Man, Z. L. Kong, Z. K. Lin, G. Duan, N. Chen, and B. Xia, Observation of fractal higher-order topological states in acoustic metamaterials, Sci. Bull. **67,** 2069 (2022).

[47] J. Li, Q. Mo, J. H. Jiang, and Z. Yang, Higher-order topological phase in an acoustic fractal lattice, Sci. Bull. **67,** 2040 (2022).

[48] S. Imhof, C. Berger, F. Bayer, J. Brehm, L. W. Molenkamp, T. Kiessling, and R. Thomale, Topolectrical-circuit realization of topological corner modes, Nat. Phys. **14,** 925 (2018).

[49] M. Ezawa, Higher-order topological electric circuits and topological corner resonance on the breathing kagome and pyrochlore lattices, Phys. Rev. B **98,** 201402 (2018).

[50] J. Bao, D. Zou, W. Zhang, W. He, H. Sun, and X. Zhang, Topoelectrical circuit octupole insulator with topologically protected corner states, Phys. Rev. B **100,** 201406 (2019).

[51] J. Wu, X. Huang, J. Lu, Y. Wu, W. Deng, F. Li, and Z. Liu, Observation of corner states in second-order topological electric circuits, Phys. Rev. B **102,** 104109 (2020).

[52] H. Yang, Z. X. Li, Y. Liu, Y. Cao, and P. Yan, Observation of symmetry-protected zero modes in topolectrical circuits, Phys. Rev. Res. **2,** 022028 (2020).

[53] L. Song, H. Yang, Y. Cao, and P. Yan, Realization of the square-root higher-order topological insulator in electric circuits, Nano Lett. **20,** 7566 (2020).

[54] S. Liu, S. Ma, Q. Zhang, L. Zhang, C. Yang, O. You, W. Gao, Y. Xiang, T. J. Cui, and S. Zhang, Octupole corner state in a three-dimensional topological circuit, Light Sci. Appl. **9,** 145 (2020).

[55] W. Zhang, D. Zou, J. Bao, W. He, Q. Pei, H. Sun, and X. Zhang, Topolectrical-circuit realization of a four-dimensional hexadecapole insulator, Phys. Rev. B **102,** 100102 (2020).

[56] W. Zhang, D. Zou, Q. Pei, W. He, J. Bao, H. Sun, and X. Zhang, Experimental observation of higher-order topological Anderson insulators, Phys. Rev. Lett. **126,** 146802 (2021).

[57] B. Lv, R. Chen, R. Li, C. Guan, B. Zhou, G. Dong, C. Zhao, Y. Li, Y. Wang, H. Tao, J. Shi, and D.-H. Xu, Realization of quasicrystalline quadrupole topological insulators in electrical circuits, Commun. Phys. **4,** 108 (2021).

[58] S. S. Yamada, T. Li, M. Lin, C. W. Peterson, T. L. Hughes, and G. Bahl, Bound states at partial dislocation defects in multipole higher-order topological insulators, Nat. Commun. **13,** 2035 (2022).

[59] N. A. Olekhno, A. D. Rozenblit, V. I. Kachin, A. A. Dmitriev, O. I. Burmistrov, P. S. Seregin, D. V. Zhirihin, and M. A. Gorlach, Experimental realization of topological corner states in long-range-coupled electrical circuits, Phys. Rev. B **105,** L081107 (2022).

[60] W. Zhang, H. Yuan, N. Sun, H. Sun, and X. Zhang, Observation of novel topological states in hyperbolic lattices, Nat. Commun. **13,** 2937 (2022).

[61] H. Yang, L. Song, Y. Cao, and P. Yan, Observation of type-III corner states induced by long-range interactions, Phys. Rev. B **106,** 075427 (2022).

[62] X. Zheng, T. Chen, and X. Zhang, Topolectrical circuit realization of quadrupolar surface semimetals, Phys. Rev. B **106,** 035308 (2022).

[63] H. R. Kim, M. S. Hwang, D. Smirnova, K. Y. Jeong, Y. Kivshar, and H. G. Park, Multipolar lasing modes from topological corner states, Nat. Commun. **11,** 5758 (2020).

[64] W. Zhang, X. Xie, H. Hao, J. Dang, S. Xiao, S. Shi, H. Ni, Z. Niu, C. Wang, K. Jin, X. Zhang, and X. Xu, Low-threshold topological nanolasers based on the second-order corner state, Light Sci. Appl. **9,** 109 (2020).

[65] F. Zangeneh-Nejad and R. Fleury, Nonlinear second-order topological insulators, Phys. Rev. Lett. **123,** 053902 (2019).

[66] M. S. Kirsch, Y. Zhang, M. Kremer, L. J. Maczewsky, S. K. Ivanov, Y. V. Kartashov, L. Torner, D. Bauer, A. Szameit, and M. Heinrich, Nonlinear second-order photonic topological insulators, Nat. Phys. **17,** 995 (2021).

[67] Z. Hu, D. Bongiovanni, D. Jukić, E. Jajtić, S. Xia, D. Song, J. Xu, R. Morandotti, H. Buljan, and Z. Chen, Nonlinear control of photonic higher-order topological bound states in the continuum, Light Sci. Appl. **10,** 164 (2021).

[68] M. Ezawa, Nonlinear non-Hermitian higher-order topological laser, Phys. Rev. Res. **4,** 013195 (2022).

[69] X. Xie, W. Zhang, X. He, S. Wu, J. Dang, K. Peng, F. Song, L. Yang, H. Ni, Z. Niu, C. Wang, K. Jin, X. Zhang, and X. Xu, Cavity quantum electrodynamics with second-order topological corner state, Laser Photonics Rev. **14,** 1900425 (2020).

[70] C. Li, M. Li, L. Yan, S. Ye, X. Hu, Q. Gong, and Y. Li, Higher-order topological biphoton corner states in two-dimensional photonic lattices, Phys. Rev. Res. **4,** 023049 (2022).

[71] W. A. Benalcazar and A. Cerjan, Chiral-symmetric higher-order topological phases of matter, Phys. Rev. Lett. **128,** 127601 (2022).

[72] C. H. Lee, S. Imhof, C. Berger, F. Bayer, J. Brehm, L. W. Molenkamp, T. Kiessling, and R. Thomale, Topolectrical circuits, Commun. Phys. **1,** 39 (2018).

[73] E. Zhao, Topological circuits of inductors and capacitors, Ann. Phys. **399,** 289 (2018).

[74] J. Dong, V. Juričić, and B. Roy, Topolectric circuits: Theory and construction, Phys. Rev. Res. **3,** 023056 (2021).

[75] P. M. Lenggenhager, A. Stegmaier, L. K. Upreti, T. Hofmann, T. Helbig, A. Vollhardt, M. Greiter, C. H. Lee, S. Imhof, H. Brand, T. Kießling, I. Boettcher, T. Neupert, R. Thomale, and T. Bzdušek, Simulating hyperbolic space on a circuit board, Nat. Commun. **13,** 4373 (2022).

[76] W. Zhang, F. Di, X. Zheng, H. Sun, and X. Zhang, Hyperbolic band topology with non-trivial second Chern numbers, Nat. Commun. **14,** 1083 (2023).

[77] A. Chen, H. Brand, T. Helbig, T. Hofmann, S. Imhof, A. Fritzsche, T. Kießling, A. Stegmaier, L. K. Upreti, T. Neupert, T. Bzdušek, M. Greiter, R. Thomale, and I. Boettcher, Hyperbolic matter in electrical circuits with tunable complex phases, Nat. Commun. **14,** 622 (2023).

[78] Y. Wang, H. M. Price, B. Zhang, and Y. D. Chong, Circuit implementation of a four-dimensional topological insulator, Nat. Commun. **11,** 2356 (2020).

[79] X. Zheng, T. Chen, W. Zhang, H. Sun, and X. Zhang, Exploring topological phase transition and Weyl physics in five dimensions with electric circuits, Phys. Rev. Res. **4,** 033203 (2022).

[80] J. Wu, Z. Wang, Y. Biao, F. Fei, S. Zhang, Z. Yin, Y. Hu, Z. Song, T. Wu, F. Song, and R. Yu, Non-Abelian gauge fields in circuit systems, Nat. Electron. **5,** 635 (2022).

[81] Z. Wang, X. T. Zeng, Y. Biao, Z. Yan, and R. Yu, Realization of a Hopf insulator in circuit systems, Phys. Rev. Lett. **130,** 057201 (2023).

[82] Y. Hadad, J. C. Soric, A. B. Khanikaev, and A. Alu, Self-induced topological protection in nonlinear circuit arrays, Nat. Electron. **1,** 178 (2018).

[83] Y. Wang, L. J. Lang, C. H. Lee, B. Zhang, and Y. D. Chong, Topologically enhanced harmonic generation in a nonlinear transmission line metamaterial, Nat. Commun. **10,** 1102 (2019).

[84] T. Helbig, T. Hofmann, S. Imhof, M. Abdelghany, T. Kiessling, L. W. Molenkamp, C. H. Lee, A. Szameit, M. Greiter, and R. Thomale, Generalized bulk-boundary correspondence in non-Hermitian topolectrical circuits, Nat. Phys. **16**, 747 (2020).

[85] A. Stegmaier, S. Imhof, T. Helbig, T. Hofmann, C. H. Lee, M. Kremer, Al. Fritzsche, T. Feichtner, S. Klembt, S. Höfling, I. Boettcher, I. C. Fulga, L. Ma, O. G. Schmidt, M. Greiter, T. Kiessling, A. Szameit, and R. Thomale, Topological defect engineering and $\mathcal{PT}$ symmetry in non-Hermitian electrical circuits, Phys. Rev. Lett. **126**, 215302 (2021).

[86] D. Zou, T. Chen, W. He, J. Bao, C. H. Lee, H. Sun, and X. Zhang, Observation of hybrid higher-order skin-topological effect in non-Hermitian topolectrical circuits, Nat. Commun. **12**, 7201 (2021).

[87] N. Pan, T. Chen, H. Sun, and X. Zhang, Electric-circuit realization of fast quantum search, Research **2021**, 9793071 (2021).

[88] H. Zhang, T. Chen, N. Pan, and X. Zhang, Electric-circuit simulation of quantum fast hitting with exponential speedup, Adv. Quantum Technol. **5**, 2100143 (2022).

[89] D. Zou, N. Pan, T. Chen, H. Sun, and X. Zhang, Experimental simulation of topological quantum computing with classical circuits, Adv. Intell. Syst. **5**, 2300354 (2023).

[90] A. Stegmaier, H. Brand, S. Imhof, A. Fritzsche, T. Helbig, T. Hofmann, and L. K. Upreti, Realizing efficient topological temporal pumping in electrical circuits, arXiv:2306.15434 (2023).

[91] T. Kotwal, F. Moseley, A. Stegmaier, S. Imhof, H. Brand, T. Kießling, R. Thomale, H. Ronellenfitsch, and J. Dunkel, Active topolectrical circuits, Proc. Natl. Acad. Sci. **118**, e2106411118 (2021).

[92] P. Zhu, X. Q. Sun, T. L. Hughes, and G. Bahl, Higher rank chirality and non-Hermitian skin effect in a topolectrical circuit, Nat. Commun. **14**, 720 (2023).

[93] See the Supplemental Material at http://link.aps.org/supplemental/10.1103/PhysRevApplied.20.064042 for details of the implementation in electrical circuits and grounding setting; the circuit and method for LDOS measurements; the measured LDOS data for all sites; the discrepancy analysis for simulated and measured LDOS; the LDOS distributions for $N = 2, 3$ systems; and the decay lengths of the corner modes.

[94] C. W. Peterson, T. Li, W. A. Benalcazar, T. L. Hughes, and G. Bahl, A fractional corner anomaly reveals higher-order topology, Science **368**, 1114 (2020).

[95] C. W. Peterson, T. Li, W. Jiang, T. L. Hughes, and G. Bahl, Trapped fractional charges at bulk defects in topological insulators, Nature **589**, 376 (2021).

[96] Y. Liu, S. Leung, F. F. Li, Z. K. Lin, X. Tao, Y. Poo, and J. H. Jiang, Bulk-disclination correspondence in topological crystalline insulators, Nature **589**, 381 (2021).

[97] C. P. Liang, Y. Liu, F. F. Li, S. W. Leung, Y. Poo, and J. H. Jiang, Fractional topological numbers at photonic edges and corners, Phys. Rev. Appl. **20**, 034028 (2023).

[98] B. Xie, R. Huang, S. Jia, Z. Lin, J. Hu, Y. Jiang, S. Ma, P. Zhan, M. Lu, Z. Wang, Y. Chen, and S. Zhang, Bulk-local-density-of-state correspondence in topological insulators, Nat. Commun. **14**, 7347 (2023).

[99] H. Ge, Z. W. Long, X. Y. Xu, J. G. Hua, Y. Liu, B. Y. Xie, J.-H. Jiang, M.-H. Lu, and Y.-F. Chen, Direct measurement of acoustic spectral density and fractional topological charge, Phys. Rev. Appl. **19**, 034073 (2023).

[100] W. A. Benalcazar, J. Noh, M. Wang, S. Huang, K. P. Chen, and M. C. Rechtsman, Higher-order topological pumping and its observation in photonic lattices, Phys. Rev. B **105**, 195129 (2022).

[101] B. Y. Xie, O. You, and S. Zhang, Photonic topological pump between chiral disclination states, Phys. Rev. A **106**, L021502 (2022).

[102] O. You, S. Liang, B. Xie, W. Gao, W. Ye, J. Zhu, and S. Zhang, Observation of non-Abelian Thouless pump, Phys. Rev. Lett. **128**, 244302 (2022).

[103] A. Rüegg and C. Lin, Bound states of conical singularities in graphene-based topological insulators, Phys. Rev. Lett. **110**, 046401 (2013).1

[104] J. C. Teo and T. L. Hughes, Existence of Majorana-fermion bound states on disclinations and the classification of topological crystalline superconductors in two dimensions, Phys. Rev. Lett. **111**, 047006 (2013).

[105] T. Li, P. Zhu, W. A. Benalcazar, and T. L. Hughes, Fractional disclination charge in two-dimensional C_n-symmetric topological crystalline insulators, Phys. Rev. B **101**, 115115 (2020).

[106] R. El-Ganainy, K. G. Makris, M. Khajavikhan, Z. H. Musslimani, S. Rotter, and D. N. Christodoulides, Non-Hermitian physics and PT symmetry, Nat. Phys. **14**, 11 (2018).

[107] C. M. Bender and S. Boettcher, Real spectra in non-Hermitian Hamiltonians having $\mathcal{PT}$ symmetry, Phys. Rev. Lett. **80**, 5243 (1998).